PAPER

Check for updates

Removal of aqueous Hg(II) by thiol-functionalized nonporous silica microspheres prepared by one-step sol–gel method

Ruixue Liang and Hua Zou [ID] *

It is well known that thiol-functionalized silica (SiO_2-SH) can be used as an effective adsorbent for the removal of Hg(II) from water. Studies in this field have focused on porous silica gels and mesoporous silicas that have large surface area and pore volume, while nonporous silica particles are seldom reported. This work aims to investigate the Hg(II) adsorption properties of nonporous SiO_2-SH microspheres prepared by a simple one-step sol–gel method. The effects of pH, initial concentration of Hg(II) and temperature on the adsorption properties of the SiO_2-SH microspheres were studied via batch adsorption experiments. The maximum adsorption capacity for Hg(II) at 293 K calculated from the Langmuir equation was 377.36 mg g^{-1}. The adsorption kinetics and equilibrium data were well-fitted to the pseudo-second-order model and the Langmuir isotherm model, respectively.

1 Introduction

Hg(II) is the common form of mercury, which is one of the most toxic heavy metals existing in the environment. The origins of mercury contamination can be natural and anthropogenic, more commonly the latter. The natural sources typically involve mercury from volcanic activity and weathering of rocks; while the anthropogenic sources include coal-fired power generation, industrial production, waste incineration, mining, *etc.* The mercury can accumulate in the water environment on which humans depend for survival. After being ingested by the human body, it will accumulate in certain organs, causing chronic poisoning.[1]

In the past decades, various techniques for the removal of Hg(II) (*e.g.* ion exchange, solvent extraction, adsorption, precipitation) have been developed.[2,3] Among them, adsorption is widely used because adsorbent is easy to be operated and cost-effective. Various adsorbents such as activated carbons, silica gel, mesoporous silica, conjugated polymers, and biomass have been reported for Hg(II) removal.[4–7] These materials generally carry sulfur- and nitrogen-containing functional groups on the surface, which show a high affinity for Hg(II). For example, the thiol group is an excellent ligand that can exhibit remarkable interaction to Hg(II) due to the soft Lewis acid–base interactions (thiol group is a soft Lewis base and mercury is a soft Lewis acid).[8] On the other hand, silica offers some advantages such as good mechanical strength, good thermal stability and ease of recovery.[9–11] Therefore, thiol-functionalized

School of Materials Science and Engineering, University of Shanghai for Science and Technology, 516 Jungong Road, Shanghai 200093, China. E-mail: hua.zou@usst.edu.cn

silica (SiO_2-SH) has been widely studied as an effective adsorbent for the removal of Hg(II) from water.[12–40] So far, studies in this field have focused on porous SiO_2-SH gel,[12–16] mesoporous SiO_2-SH microspheres[17–33] and mesoporous SiO_2-SH microspheres with magnetic cores[34–39] that have large surface area and pore volume. However, nonporous SiO_2-SH microsphere as Hg(II) adsorbent is seldom reported, although we note that there are two reports on Fe_3O_4@SiO_2-SH particles for Hg(II) adsorption, in which the silica is nonporous.[40,41] In this context, it is perhaps also noteworthy that there are several reports on amino-functionalized,[42] polypyrrole-functionalized,[43] and ethylenediaminetetraacetic acid-functionalized[44] $CoFe_2O_4$@SiO_2 microspheres with nonporous silica shell for Hg(II) removal.

On the other hand, it is interesting to note that the number of functional groups on the absorbent surface might be more important than large surface area and pore volume, which means nonporous microsphere is also promising for heavy metal adsorption providing there are abundant functional groups on its surface. For example, Qu *et al.* prepared nonporous silica particles functionalized with rich sulfonic acid groups and used them for adsorbing heavy metals. It is shown that the adsorption capacity of Pb(II) could reach to 635 mg g^{-1} although the surface area of the adsorbent was only 1.58 m^2 g^{-1}.[45] The strong adsorption ability of the sulfonic acid functionalized silica microspheres was attributed to the nonporous particles with rich sulfonic groups which facilitated the mass transport of metal ions to the active sites.

In principle, surface-modified silica microspheres can be fabricated through two common methods.[46] One method is based on silanization of preformed silica microspheres with silane-coupling agents in a dried organic solvent or aqueous media, leading to monolayer or multilayer modification,

respectively. However, this two-step method suffers from harsh experimental conditions (for monolayer modification) or low reproducibility (for multilayer modification). Another method involves a one-step co-condensation reaction of an organosilane and a tetraalkoxysilane precursor, in which both the size and shape of the hybrid silica spheres were much less controlled. Alternatively, hybrid silica spheres could be fabricated by using a suitable silane as the sole precursor in aqueous solution. This method is particularly suitable to prepare SiO_2-SH microspheres from (3-mercaptopropyl)trimethoxysilane (MPTMS) precursor since it can easily self-hydrolyze into organosilanetriol owing to its molecular structure: there are three short carbon chains in the MPTMS molecule, which are suitable for changing from alkoxy groups to hydroxy groups.[47] In addition, methanol is released during the hydrolysis reaction, which can promote dissolution of MPTMS in water.

Compared with porous SiO_2-SH gel and mesoporous SiO_2-SH spheres, nonporous SiO_2-SH microspheres may offer the advantages of easier adsorption and desorption as the active sites are located on the surface. This study aims to investigate the Hg(II) adsorption properties of the nonporous SiO_2-SH microspheres prepared by the one-step sol–gel method. The SiO_2-SH microspheres were extensively characterized by laser diffraction instrument, SEM, TEM, nitrogen adsorption–desorption analyzer, FTIR, Raman spectroscopy, XPS and TGA. The isotherm, kinetics and mechanism of Hg(II) adsorbed by the SiO_2-SH microspheres were studied by a series of batch experiments. Finally, the resorption property of the adsorbent was also investigated. As far as we are aware, this is the first time that nonporous SiO_2-SH microsphere is reported as Hg(II) adsorbent.

2   Experimental

2.1   Materials

MPTMS (95%) and ammonium hydroxide solution (25%) were purchased from Sigma-Aldrich. Ethanol ($\geq$99.7%), sodium hydroxide ($\geq$96%), hydrochloric acid (36–38%), and nitric acid (65–68%) were supplied by Sinopharm Chemical Reagent Co., Ltd. $Hg(NO_3)_2 \cdot H_2O$ standard solution (1000 µg mL^{-1}, in 1.0 mol L^{-1} HNO$_3$) was provided by General Research Institute for Nonferrous Metals, Beijing, China. All chemicals were used as received and all water used was deionized.

2.2   Synthesis of SiO₂-SH microspheres

The SiO_2-SH microspheres were prepared using a one-step method through the self-hydrolysis of organosilane in aqueous solution. MPTMS (2.0 g) was dissolved in water (100 g) in a single-necked round bottom flask equipped with a magnetic stir bar under vigorous stirring. Once a transparent solution was obtained, NH$_4$OH (3.4 mL) was added to the solution and the reaction was allowed to proceed for 4 h. The resulting microspheres were then purified by repeated centrifugation and redispersion cycles, replacing supernatants with ethanol, ethanol/water mixture (1 : 1) and H$_2$O, respectively. Finally, the microspheres were redispersed in water by repeated

ultrasonication for a few hours. High temperature was avoided during the ultrasonic treatment process by the addition of ice. Drying the microspheres to powder form was also avoided for adsorption studies, since this would result in aggregation of the SiO_2-SH microspheres and also make redispersion of the particles more difficult.

2.3   Characterization

The morphology of the SiO_2-SH microspheres was observed by scanning electron microscopy (SEM, Quanta FEG 450) and transmission electron microscopy (TEM, FEI Tecnai G2 F30). The SEM samples were prepared on double-sided adhesive carbon disks and sputter-coated with gold, and the TEM samples were prepared on carbon-coated copper grids. The size and size distribution of the SiO_2-SH microspheres were determined by laser diffraction using Malvern Mastersizer 2000. The measurement was conducted in triplicate on highly dilute aqueous dispersion. The nitrogen adsorption–desorption measurement of the SiO_2-SH microspheres was performed using a Micromeritics ASAP 2460 instrument and the pore volume was calculated by the BJH equation. FTIR spectra were recorded on a PerkinElmer Spectrum 100 FTIR spectrometer from KBr disks. A laser Raman spectrometer (IK3301R-G) was used to obtain a Raman spectrum of the microspheres. X-ray photoelectron spectroscopy (XPS, Versa Probe PHI-5000, ULVAC-PHI Inc., Japan) was used to detect the surface composition of the sample. TGA experiments were carried out using a PerkinElmer Pyris 1 TGA instrument in N$_2$ at a heating rate of 10 °C min^{-1} from room temperature to 800 °C. The concentration of heavy metal ion was determined by inductively coupled plasma atomic emission spectrometry (ICP-AES, PerkinElmer Optima 7000DV). A Ray magnetic PHS-3C pH meter was used for pH measurements.

2.4   Adsorption experiments

The adsorption experiments were first carried out in the pH range of 2.5 to 6.5 as follows. The appropriate amount of the SiO_2-SH microsphere dispersion (equivalent to 5 mg of dry SiO_2-SH) was diluted into 25 mL aqueous dispersion at desired pH containing 5 mg of Hg(II), followed by stirring (280 rpm, 293 K) for 24 h prior to filtration. The equilibrium concentration of the Hg(II) in aqueous solution was determined by ICP-AES. The adsorption capacity (Q_e, mg g^{-1}) was calculated using the following equation:

$$Q_e = \frac{(C_0 - C_e)}{W} V \qquad (1)$$

where C_0 (mg L^{-1}) is the initial concentration of Hg(II) in solution, C_e (mg L^{-1}) is the equilibrium concentration, V (L) is the volume of the solution, and W (g) is the mass of dry SiO_2-SH microspheres.

The adsorption kinetic experiments were conducted at 293 K, 303 K and 313 K, respectively. In each case, 200 mg L^{-1} of Hg(II) solution was set as the initial concentration of Hg(II) solution and the contact time ranged from 0 to 5 h. The adsorption isotherm study was done at 293 K, with the initial concentration of Hg(II) solution varying from 50 mg L^{-1} to 250 mg L^{-1}.

2.5 Resorption experiments

Immediately after adsorption, the SiO$_2$-SH microspheres were filtrated from the suspension and slightly washed with deionized water. The Hg-loaded microspheres were then agitated with HCl or HNO$_3$ solution (0.5–3.0 mol L^{-1}) for 24 h at room temperature followed by separation. Subsequently, the SiO$_2$-SH microspheres were reused for adsorption in the succeeding cycle.

3 Results and discussion

3.1 Characterization of SiO$_2$-SH microspheres

SiO$_2$-SH microspheres were successfully synthesized *via* self-hydrolysis of MPTMS in aqueous solution as described by Lee and coworkers.[47] The as-synthesized SiO$_2$-SH microspheres were highly functionalized but could be redispersed in water with the aid of an ultrasonic bath, which was essential for subsequent adsorption studies. The laser diffraction confirmed that the SiO$_2$-SH microspheres had a diameter of ∼1.2 μm with a relatively narrow size distribution (see Fig. 1). The relatively large size of the microspheres may be at least partially responsible for the moderate aqueous dispersibility. SEM and TEM studies indicated that the microspheres were spherical and had a smooth surface morphology (see Fig. 2). BET results showed that the microspheres were nonporous.

FTIR study (see Fig. 3) confirmed the formation of SiO$_2$-SH microspheres, since two strong Si–O–Si stretching vibration bands were observed at 1035 and 1120 cm^{-1}; these bands were different to the spectrum of pure silica (only one peak at ∼1100 cm^{-1}) because Si–C bond in the hybrid silica disrupted the symmetry of Si–O–Si structure. According to the literature,[48] the –OH groups in the hybrid silica give rise to a broad stretching vibration in the range of 3100–3700 cm^{-1}. This feature was also observed, indicating the existence of silanol groups in the SH microspheres spheres. A weak band ascribed to SH group was discernible at 2554 cm^{-1}. This is in reasonable agreement with the literature.[38,41,46] It is noteworthy that the two weak peaks of –SH at ∼2360 cm^{-1} due to the aggregation of thiol groups and the hydrogen binding effects were not found,[35,38] indicating the thiol groups in our work were non-aggregated. Raman spectroscopy, a complementary tool to FTIR spectroscopy, was also used to characterize the SiO$_2$-SH microspheres. As shown in Fig. 4, the strong characteristic stretching vibration of CH$_2$ (2916 cm^{-1}) and SH (2568 cm^{-1}) further confirmed the presence of thiol groups on the hybrid silica
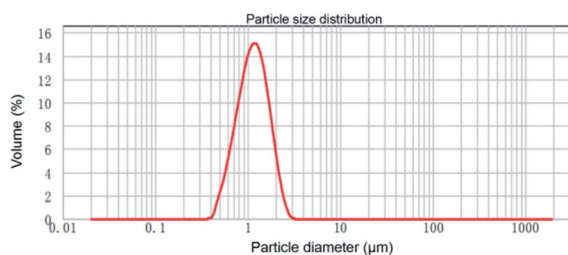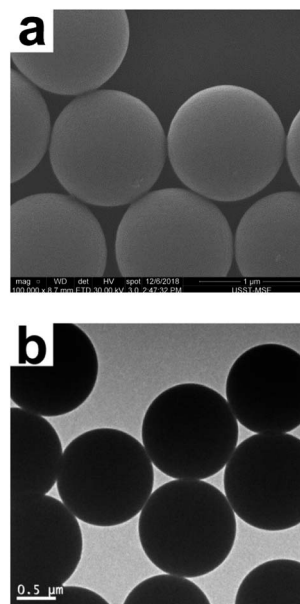

Fig. 2 (a) SEM and (b) TEM images of SiO$_2$-SH microspheres.
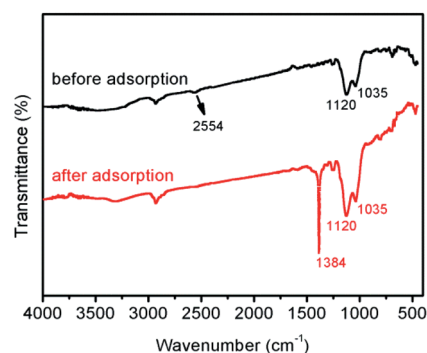

Fig. 3 FTIR spectra of SiO$_2$-SH microspheres before and after adsorption (adsorption conditions: SiO$_2$-SH 10 mg, $C_0 = 200$ mg L^{-1}, pH = 5.5, $T = 293$ K, $t = 24$ h).

microspheres.[49] It should be mentioned that the characteristic peak of S–S bond (∼509 cm^{-1}) was not observed, suggesting that the air oxidation of the thiol groups did not occur substantially.[50–53] This perhaps could be explained by the fact that the SiO$_2$-SH microspheres in this work were prepared in wet state and kept as aqueous dispersion prior to use. The surface composition of the SiO$_2$-SH microspheres was measured by XPS with a typical sampling depth of 2–10 nm, which also provided good evidence that these microspheres were sulfur-rich at their surface: the atomic content of S 2p was determined to be 7.17%.

3.2 Effect of pH on the adsorption capability

The first parameter examined in the adsorption process was the solution pH. In view of the fact that Hg(II) may precipitate in alkaline aqueous solution, the study was carried out in the pH range of 2.5–6.5. As shown in Fig. 5, the adsorption capacity of SiO$_2$–OH for Hg(II) increased rapidly with increasing pH from

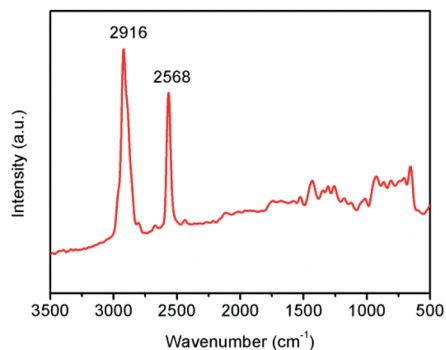Fig. 1 Particle size distribution histogram of SiO$_2$-SH microspheres.

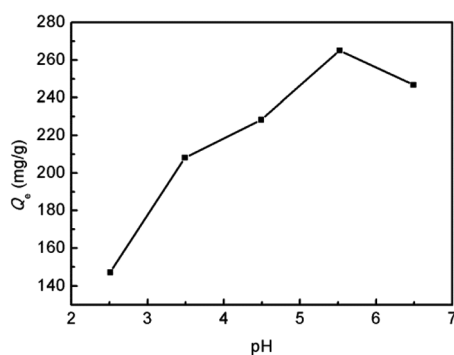Fig. 4 Raman spectrum of SiO_2-SH microspheres.

Fig. 5 Effect of solution pH on the adsorption capacity of SiO_2-SH microspheres for Hg(II) (SiO_2-SH 5 mg, C_0 = 200 mg L^{-1}, pH 2.5–6.5, T = 293 K, t = 24 h).

2.5 to 5.5. However, a further increase of pH value to 6.5 resulted in a slight reduction of adsorption capacity. At pH 5.5, SiO_2-SH microspheres showed the highest adsorption capacity of 265.1 mg g^{-1}. Similar results have been reported in the literature on Hg(II) adsorption.[4] In this context, we note that the adsorption of Hg(II) onto the surface of SiO_2-SH substrates is well-documented.[21,27,38,41] As shown in Fig. 6, there might be three forms of Hg(II) in aqueous solution: Hg^{2+}, $Hg(OH)^+$ and $Hg(OH)_2$. At lower pH (pH < 3), Hg^{2+} is the dominating specie, and its amount decreases with increasing solution pH until disappearance. In contrast, the amount of $Hg(OH)^+$ and $Hg(OH)_2$ increases with increasing solution pH. The
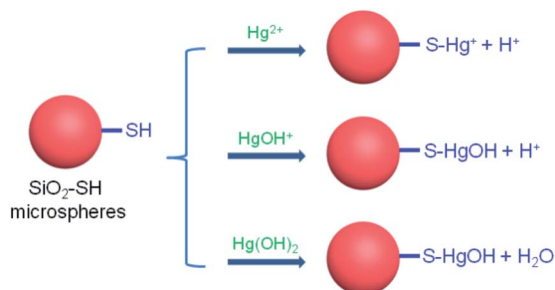
complexation between the thiol group and Hg^{2+} generates positive $S–Hg^+$ specie, which may prevents, to some extent, further Hg^{2+} adsorption due to electrostatic repulsive forces. In addition, since SiO_2 has a negative zeta potential over a wide range of pH (typically from pH 2 to pH 12) due to the presence of silanol groups, there may be also an electrostatic interaction between the positively charged Hg^{2+} and the negatively charged SiO_2-SH microsphere surface.[31,36] The amount of $Hg(OH)^+$ species has a maximum value at pH ~ 4.0 and the amount of $Hg(OH)_2$ species becomes dominant at higher pH (pH > 6), both of which can be adsorbed by thiol group without electrostatic repulsion. In the following discussion, the adsorption experiments were conducted at pH 5.5.

3.3 FTIR and XPS analysis of the Hg(II)-loaded SiO_2-SH microspheres

The adsorption of Hg(II) on the surfaces of SiO_2-SH microspheres was investigated by FTIR and XPS. FTIR study confirmed Hg(II) adsorption (see Fig. 3), since an obvious characteristic peak of nitrate appeared at 1384 cm^{-1} after adsorption as $Hg(NO_3)_2$ was used as the source for Hg(II).[6] In addition, the peak at 2554 cm^{-1} (S–H stretching vibration) disappeared after adsorption while other peaks were essentially unchanged, suggesting that only S–H participated in the adsorption process.

XPS survey spectra of the microspheres before and after adsorption are shown in Fig. 7a. The presence of Hg 4f signal after adsorption provided further evidence that Hg(II) was adsorbed onto the SiO_2-SH microspheres although the position of the Hg 4f signal overlapped with that of Si 2p in the overview spectrum.[52] The Hg atomic content is 2.46% after adsorption. Furthermore, for the S 2p spectrum, there are a significant decrease in intensity and a shift of binding energy from 163.42 to 163.47 eV after adsorption (see Fig. 7b). This is probably due to the donation of the electrons from the S atoms to Hg(II), indicating that a complex between S and Hg formed.[37,39] Fig. 7d
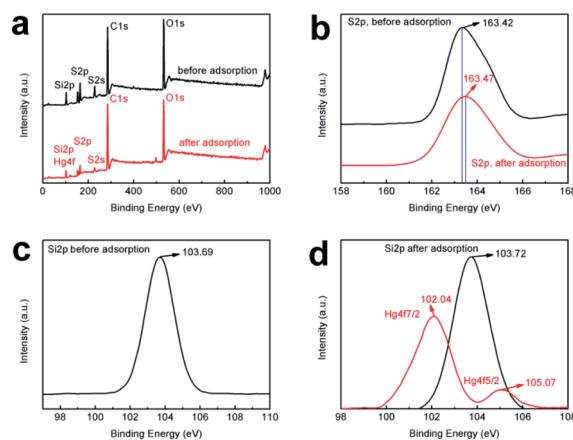

Fig. 6 Possible adsorption mechanism of Hg(II) onto the surface of SiO_2-SH microspheres.

Fig. 7 XPS survey spectra recorded for the SiO_2-SH microspheres: (a) before and after adsorption (adsorption conditions: SiO_2-SH 10 mg, C_0 = 200 mg L^{-1}, pH = 5.5, T = 293 K, t = 24 h), (b) S 2p before and after adsorption, (c) Si 2p before adsorption, and (d) Si 2p/Hg 4f after adsorption.
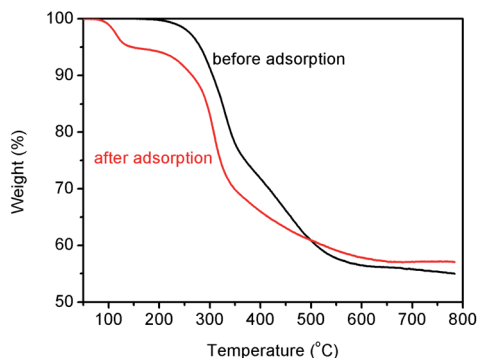
Fig. 8 TGA curves of the SiO$_2$-SH microspheres before and after Hg(II) adsorption (adsorption conditions: SiO$_2$-SH 10 mg, C_0 = 200 mg L^{-1}, pH = 5.5, T = 293 K, t = 24 h).

shows the high-resolution Hg 4f spectrum of the sample after Hg(II) adsorption, which has two peaks at 102.04 eV and 105.07 eV, respectively. In comparison with Fig. 7c, it was obvious that Hg(II) was adsorbed through the binding between S and Hg(II).

3.4 Thermal stability

The TGA curves for the SiO$_2$-SH microspheres before and after adsorption of Hg(II) are shown in Fig. 8. When the temperature is lower than 200 °C, the SiO$_2$-SH microspheres showed an excellent thermal stability. The microspheres had a ∼56.5 wt% of residue when heated to 600 °C. The observed one sharp mass loss was attributed to the pyrolysis of the organic components of the hybrid silica microspheres, which indicated that the microspheres contained a large number of organic groups (including thiol groups).[54] For the SiO$_2$-SH microspheres after Hg(II) adsorption, there was an additional decomposition step in the range of 100–150 °C, which might be related to the desorption of the residual water and –NO$_3$ groups bonded to the microspheres. It seemed the thermal stability of the Hg(II)-loaded SiO$_2$-SH microspheres was lowered. However, they had a slightly higher residual weight of 57.8 wt% at 600 °C. This suggested that the interaction between the SiO$_2$-SH microspheres and Hg(II) led to the formation a more stable complex.
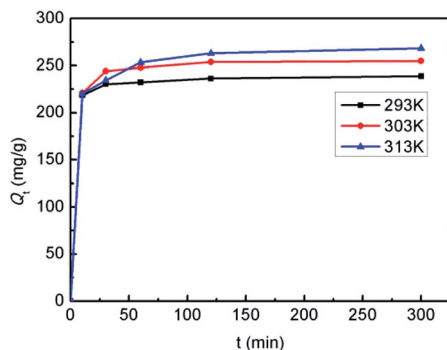
3.5 Adsorption kinetics

To better understand the adsorption process, the adsorption kinetics was studied at 293, 303 and 313 K, respectively. As shown in Fig. 9, at all temperatures, the adsorption capacities for Hg(II) increased extremely rapidly during the initial 10 min, and then increased slowly with increasing time up to 2 h. The rapid adsorption rate in the early state might be ascribed to the easy access of Hg(II) to the active sites on the nonporous microspheres, as well as the availability of abundant vacant sites.[27] Thereafter they remained constant, which indicated that the adsorption reached equilibrium within 2 h. Furthermore, it is shown that the adsorption capacities increased with increasing temperature, suggesting that the adsorption process is temperature-dependent.

The adsorption kinetics was further examined with pseudo-first-order model and pseudo-second-order model, respectively, as shown below:

Pseudo-first-order kinetic model:[55]

$$\ln(Q_e - Q_t) = \ln Q_1 - k_1 t \tag{2}$$

Pseudo-second-order kinetic model:[56]

$$\frac{t}{Q_t} = \frac{1}{k_2 Q_2^2} + \frac{1}{Q_2} t \tag{3}$$

where Q_e is the equilibrium adsorption quantity and Q_t is the adsorption quantity at a certain time (mg g^{-1}), and k_1 and k_2 are
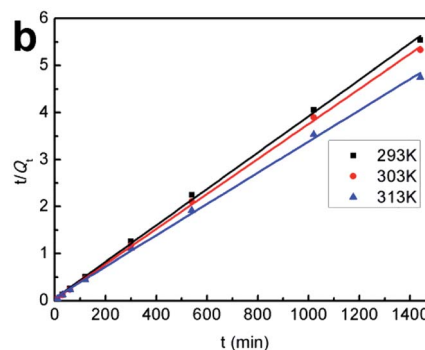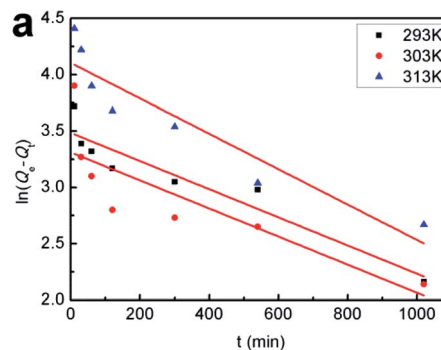

Fig. 10 (a) Pseudo-first-order kinetic model and (b) pseudo-second-order kinetic model of the SiO$_2$-SH microspheres for Hg(II) adsorption at different temperatures.

Fig. 9 Adsorption kinetic curves of the SiO$_2$-SH microspheres for Hg(II) at different temperatures (SiO$_2$-SH 10 mg, C_0 = 200 mg L^{-1}, pH 5.5).

Table 1 Kinetics model constants for adsorption of Hg(II) by SiO$_2$-SH microspheres

| T (K) | Pseudo-first-order model | | | Pseudo-second-order model | | |
	k_1 (min^{-1})	Q_1 (mg g^{-1})	$R_1{}^2$	k_2 (g mg^{-1} min^{-1})	Q_2 (mg g^{-1})	$R_2{}^2$
293	0.0013	32.60	0.9051	2.8×10^{-4}	258.40	0.9990
303	0.0013	27.44	0.6941	3.9×10^{-4}	268.82	0.9994
313	0.0016	60.56	0.8783	1.8×10^{-4}	301.20	0.9988
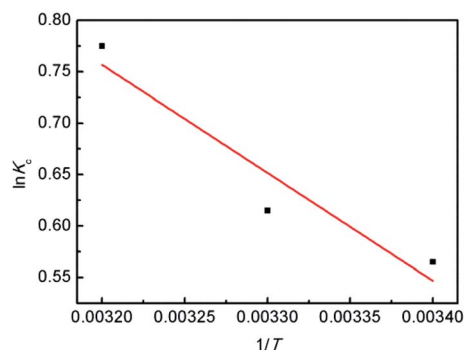
Fig. 11 Plot of ln K_c versus $1/T$ for adsorption of Hg(II) by the SiO$_2$-SH microspheres.
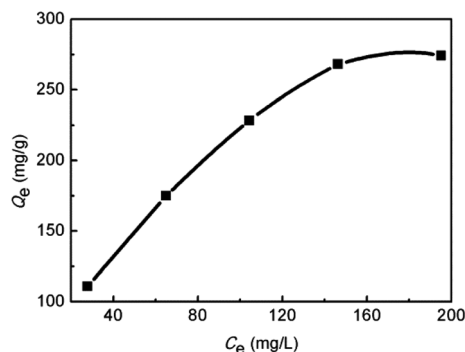
the rate constants of the pseudo-first-order model (min^{-1}) and the pseudo-second-order model (g mg^{-1} min^{-1}), respectively.

The adsorption data are fitted to eqn (2) and (3), respectively, and the results are shown in Fig. 10 and Table 1. The correlation coefficients obtained from the pseudo-second-order model are always closer to 1 and higher than those from the pseudo-first-order model, indicating that the adsorption process of SiO$_2$-SH microspheres for Hg(II) is better described by the former model and is a chemical adsorption.[7]

3.6 Adsorption thermodynamics

The adsorption thermodynamic properties were studied at 293 K, 303 K and 313 K, respectively. The Gibbs free energy (ΔG), enthalpy (ΔH), and entropy (ΔS) for the adsorption process were calculated using the following equations:

$$\ln K_c = \frac{\Delta S}{2.303R} - \frac{\Delta H}{2.303RT} \quad (4)$$

$$\Delta G = \Delta H - T\Delta S \quad (5)$$

where K_c is the distribution coefficient, R is the gas constant (8.314 J mol^{-1} K^{-1}), and T is the absolute temperature (K).

The values of ΔS and ΔH were obtained by plotting ln K_c versus $1/T$ (Fig. 11). Each value of ΔG (kJ mol^{-1}) is negative (293 K, −2.99; 303 K, −3.78; 313 K, −4.57) and less than 40 kJ mol^{-1}, suggesting that the adsorption process of Hg(II) is thermodynamically feasible and involve a chemical reaction,[39,57] which is consistent with the results obtained from the pseudo-second-order model. The positive value of $\Delta H = 20.1$ kJ mol^{-1} suggests that the Hg(II) adsorption is an endothermic process, that is, an elevated temperature may facilitate adsorption. The positive value of ΔS (78.82 J K^{-1} mol^{-1}) suggests that the adsorption is an entropy-driven process and the randomness at the solid/liquid interface is increasing.[6]

3.7 Adsorption isotherm

The adsorption isotherm was studied based on the data collected under pH 5.5 at 293 K. At this pH, precipitation of

Fig. 12 Isothermal adsorption curve of the SiO$_2$-SH microspheres for Hg(II) (SiO$_2$-SH 5 mg, pH 5.5, $T = 293$ K, $t = 24$ h).
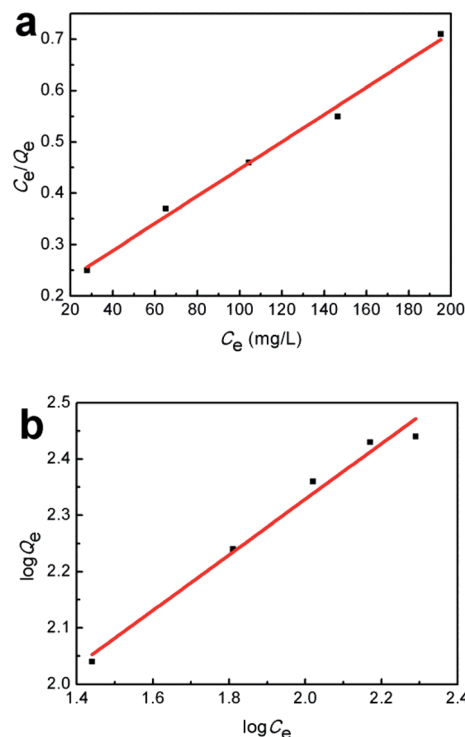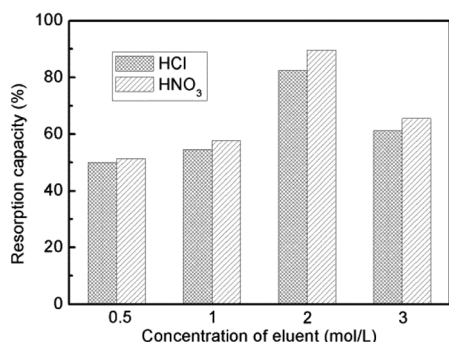

Fig. 13 (a) Langmuir and (b) Freundlich fitting curves for isothermal adsorption.

Table 2 Isothermal adsorption related parameters of the SiO$_2$-SH microspheres for Hg(II)

Langmuir			Freundlich		
Q_m (mg g^{-1})	K_L (L mg^{-1})	R^2	$1/n$	K_F ((mg g^{-1}) /(mg mL^{-1}))	R^2
377.36	0.0145	0.9935	0.49	21.94	0.9825

Fig. 14 Resorption capacity of the SiO$_2$-SH microspheres after a adsorption–desorption cycle.

Hg(II) may occur when its concentration is higher than 300 mg L^{-1}. Thus the initial Hg(II) concentrations were varied from 50 to 250 mg L^{-1}. As shown in Fig. 12, the adsorption capacity increased almost linearly with the equilibrium concentration during 30–150 mg L^{-1} (corresponding to initial Hg(II) concentration of 50–200 mg L^{-1}), and after 150 mg L^{-1} a plateau adsorption capacity of 274.1 mg g^{-1} was reached.

The adsorption isotherm was further examined by Langmuir and Freundlich models, respectively. The Langmuir isotherm model assumes that the surface properties of the adsorbent are uniform, the adsorption on the surface is monolayer adsorption, and there is no interaction between the adsorbates; while the Freundlich adsorption isotherm model assumes that the surface properties of the adsorbent are not uniform and describes the adsorption equilibrium of the heterogeneous adsorption surface. The models are shown as follows:

Langmuir equation:

$$\frac{C_e}{Q_e} = \frac{1}{Q_m K_L} + \frac{C_e}{Q_m} \tag{6}$$

Freundlich equation:

$$\log Q_e = \frac{1}{n} \log C_e + \log K_F \tag{7}$$

where C_e is the equilibrium concentration, Q_e is the equilibrium adsorption capacity of Hg(II) on the adsorbent (mg g^{-1}), Q_m is the saturated adsorption capacity based on Langmuir theory, K_L is the Langmuir adsorption constant (L mg^{-1}), and n and K_F are Freundlich constants associated with adsorption intensity and adsorption capacity, respectively.

Fig. 13 and Table 2 show the fitting curves of the Langmuir and Freundlich models, and the calculation results, respectively. By comparing the linear correlation coefficient R^2 values calculated from the two curves, it is found that the adsorption of Hg(II) by SiO$_2$-SH microspheres is in better agreement with the Langmuir adsorption, indicating that the adsorption is a monolayer process. According to the Langmuir model, the maximum adsorption capacity at 293 K was estimated to be 377.36 mg g^{-1}.

3.8 Resorption study

Resorption of the SiO$_2$-SH microspheres for Hg(II) was studied by eluting them with HCl or HNO$_3$ solution at various concentrations (0.5–3.0 mol L^{-1}), and used again for the adsorption experiment. As shown in Fig. 14, better resorption results were obtained with HNO$_3$ solution. This might be explained in terms of the affinity for Hg(II).[30] The desorption process involves disruption and loosening the S–Hg coordination complex, and the affinity of Cl$^-$ for Hg(II) is lower than that of NO$_3^-$. However, HNO$_3$ solution with higher concentration resulted in a lower resorption capacity, probably due to the partial destruction of the silica adsorbent under this condition. A maximum resorption capacity of 89.6% can be achieved with 2 mol L^{-1} HNO$_3$ solution.

3.9 Comparison to other SiO$_2$-based adsorbents

Table 3 shows the maximum Hg(II) adsorption capacity of several SiO$_2$-based adsorbents reported in the literature.[8,58] By comparison, it can be seen that the SiO$_2$-SH microspheres prepared in this work have a higher adsorption capacity (377.36 mg g^{-1} at room temperature). In addition, the microspheres have the merits of easy fabrication, rapid adsorption rate and easy to be recovered considering their relatively large

Table 3 Comparison of various SiO$_2$-based adsorbents for Hg(II) adsorption from water

Type of adsorbent	Optimal adsorption conditions	Maximum adsorption capacity (mg g^{-1})	Ref.
MPTMS-modified diatom mesoporous silica	pH 6	185.2	26
Sulfur-functionalized mesoporous silica	pH 5.8–8.2	62.3	27
Periodic mesoporous organosilica with low thiol density	pH $\sim$ 5 and 7	46.1	30
Thiol functionalization of short channel SBA-15	pH 8	195.6	31
Mesoporous Fe$_3$O$_4$@SiO$_2$-SH	pH 6.0	207.71	35
Thiol-functionalized silica	$\sim$pH 5.5	377.36	This work

size. Therefore, the SiO$_2$-SH microsphere is a type of promising material for Hg(II) removal in water.

4 Conclusions

In this study, the adsorption properties of highly monodisperse, nonporous SiO$_2$-SH microspheres prepared by a one-step sol–gel method for Hg(II) in water were studied. This simple method allows a large number of thiol groups to be created on the surface of the microspheres, which have a strong affinity to Hg(II) through Lewis acid–base interactions. The adsorption process was highly dependent on the pH, the initial concentration of Hg(II) and temperature. The isotherm data fit well to the Langmuir isotherm model, while the kinetic data followed the pseudo-second-order kinetic model, indicating that monolayer adsorption was dominant and chemisorption was the main factor for determining the rate of adsorption. At 293 K, a maximum adsorption capacity of 377.36 mg g^{-1} was estimated. Therefore, the thiol-functionalized nonporous silica is a promising adsorbent for the removal of Hg(II) from water.

Conflicts of interest

There are no conflicts to declare.

Acknowledgements

Notes and references

1 World Health Organization (WHO), https://www.who.int/en/news-room/fact-sheets/detail/mercury-and-health, accessed 18 April, 2020.

2 Q. R. Wang, D. Kim, D. D. Dionysiou, G. A. Sorial and D. Timberlake, *Environ. Pollut.*, 2004, **131**, 323–336.

3 M. D. Xia, Z. X. Chen, Y. Li, C. H. Li, N. M. Ahmad, W. A. Cheemad and S. M. Zhu, *RSC Adv.*, 2019, **9**, 20941.

4 W. Jing, B. L. Deng, H. Chen, X. R. Wang and J. Z. Zheng, *Environ. Sci. Technol.*, 2009, **43**, 5223–5228.

5 H. Cui, Y. Qian, Q. Li, Q. Zhang and J. P. Zhai, *Chem. Eng. J.*, 2012, **211–212**, 216–223.

6 X. Wang, P. F. Lv, H. Zou, Y. Li, X. Y. Li and Y. Z. Liao, *Ind. Eng. Chem. Res.*, 2016, **55**, 4911–4918.

7 H. Zou, P. F. Lv, X. Wang, D. Wu and D. G. Yu, *J. Appl. Polym. Sci.*, 2017, **134**, 44879.

8 T. Velempini and K. Pillay, *J. Environ. Chem. Eng.*, 2019, **7**, 103350.

9 E. D. E. R. Hyde, A. Seyfaee, F. Neville and R. Moreno-Atanasio, *Ind. Eng. Chem. Res.*, 2016, **55**, 8891–8913.

10 Z. Wu, H. Han, W. Han, B. Kim, K. H. Ahn and K. Lee, *Langmuir*, 2007, **23**, 7799–7803.

11 H. Zou, S. S. Wu and J. Shen, *Chem. Rev.*, 2008, **108**, 3893–3957.

12 A. Walcarius, M. Etienne and J. Bessière, *Chem. Mater.*, 2002, **14**, 2757–2766.

13 K. H. Nam, S. Gomez-Salazar and L. L. Tavlarides, *Ind. Eng. Chem. Res.*, 2003, **42**, 1955–1964.

14 M. Puanngam and F. Unob, *J. Hazard. Mater.*, 2008, **154**, 578–587.

15 K. Johari, N. Saman and H. Mat, *Environ. Technol.*, 2014, **35**, 629–636.

16 K. Johari, N. Saman and H. Mat, *Can. J. Chem. Eng.*, 2014, **92**, 1048–1058.

17 E. Da'na, *Microporous Mesoporous Mater.*, 2017, **247**, 145–157.

18 A. Bibby and L. Mercier, *Chem. Mater.*, 2002, **14**, 1591–1597.

19 A. M. Walcarius and B. Lebeau, *Chem. Mater.*, 2003, **15**, 2161–2173.

20 A. Walcarius and C. Delacôte, *Chem. Mater.*, 2003, **15**, 4181–4192.

21 A. Walcarius and C. Delacôte, *Anal. Chim. Acta*, 2005, **547**, 3–13.

22 S. J. L. Billinge, E. J. McKimmy, M. Shatnawi, H. J. Kim, V. Petkov, D. Wermeille and T. J. Pinnavaia, *J. Am. Chem. Soc.*, 2005, **127**, 8492–8498.

23 C. Delacôte, F. O. M. Gaslain, B. Lebeau and A. Walcarius, *Talanta*, 2009, **79**, 877–886.

24 F. O. M. Gaslain, C. Delacôte, A. Walcarius and B. Lebeau, *J. Sol-Gel Sci. Technol.*, 2009, **49**, 112–124.

25 A. Arencibia, J. Aguado and J. M. Arsuaga, *Appl. Surf. Sci.*, 2010, **256**, 5453–5457.

26 Y. Yu, J. Addai-Mensah and D. Losic, *Sci. Technol. Adv. Mater.*, 2012, **13**, 015008.

27 N. Saman, K. Johari and H. Mat, *Ind. Eng. Chem. Res.*, 2014, **53**, 1225–1233.

28 J. M. Arsuaga, J. Aguado, A. Arencibia and M. S. López-Gutiérrez, *Adsorption*, 2014, **20**, 311–319.

29 S. Ravi and M. Selvaraj, *Dalton Trans.*, 2014, **43**, 5299.

30 P. Figueira, M. A. O. Lourenço, E. Pereira, J. R. B. Gomes, P. Ferreira and C. B. Lopesad, *J. Environ. Chem. Eng.*, 2017, **5**, 5043–5053.

31 Y. Shen, N. Jiang, S. S. Liu, C. Zheng, X. Wang, T. Y. Huang, Y. F. Guo and R. B. Bai, *J. Environ. Chem. Eng.*, 2018, **6**, 5420–5433.

32 X. L. Yan, J. F. Meng, X. Y. Hu, R. Feng and M. Zhou, *J. Sol-Gel Sci. Technol.*, 2019, **89**, 617–622.

33 M. Kalantari, Z. Y. Gu, Y. X. Cao, C. Lei and J. Zhang, *Environ. Sci.: Nano*, 2020, **7**, 851.

34 J. Dong, Z. H. Xu and F. Wang, *Appl. Surf. Sci.*, 2008, **254**, 3522–3530.

35 G. L. Li, Z. S. Zhao, J. Y. Liu and G. B. Jiang, *J. Hazard. Mater.*, 2011, **192**, 277–283.

36 O. Hakami, Y. Zhang and C. J. Banks, *Water Res.*, 2012, **46**, 3913–3922.

37 X. Zhang, T. Wu, Y. Zhang, D. H. Ng, H. Zhao and G. Wang, *RSC Adv.*, 2015, **5**, 51446–51453.

38 H. Zhu, Y. Shen, Q. Wang, K. Chen, X. Wang, G. W. Zhang, J. J. Yang, Y. F. Guo and R. B. Bai, *RSC Adv.*, 2017, **7**, 39204.

39 Z. Z. Zhang, K. Xia, Z. W. Pan, C. X. Yang, X. Wang, G. W. Zhang, Y. F. Guo and R. B. Bai, *Appl. Surf. Sci.*, 2020, **500**, 143970.

40 S. X. Zhang, Y. Y. Zhang, J. S. Liu, Q. Xu, H. Q. Xiao, X. Y. Wang, H. Xu and J. Zhou, *Chem. Eng. J.*, 2013, **226**, 30–38.

41 Z. X. Wang, J. Xu, Y. J. Hu, H. Zhao, J. L. Zhou, Yu Liu, Z. M. Lou and X. H. Xu, *J. Taiwan Inst. Chem. Eng.*, 2016, **60**, 394–402.

42 X. Wang, Z. Z. Zhang, Y. H. Zhao, K. Xia, Y. F. Guo, Z. Qu and R. B. Bai, *Nanomaterials*, 2018, **8**, 673.

43 Y. H. Zhao, K. Xia, Z. Z. Zhang, Z. M. Zhu, Y. F. Guo and Z. Qu, *Nanomaterials*, 2019, **9**, 455.

44 K. Xia, Y. F. Guo, Q. J. Shao, Q. Zan and R. B. Bai, *Nanomaterials*, 2019, **9**, 1532.

45 Q. S. Qu, Q. Gu, Z. L. Gu, Y. Q. Shen, C. Y. Wang and X. Y. Hu, *Colloids Surf., A*, 2012, **415**, 41–46.

46 H. Zou and H. Schlaad, *J. Polym. Sci., Part A: Polym. Chem.*, 2015, **53**, 1260–1267.

47 Y. G. Lee, J. Park, C. Oh, S. Oh and Y. C. Kim, *Langmuir*, 2007, **23**, 10875–10878.

48 T. S. Deng, Q. F. Zhang, J. Y. Zhang, X. Shen, K. T. Zhu and J. L. Wu, *J. Colloid Interface Sci.*, 2009, **329**, 292–299.

49 A. Bertin and H. Schlaad, *Chem. Mater.*, 2009, **21**, 5698–5700.

50 C. M. Li, J. Liu, L. Zhang, J. Yang and Q. H. Yang, *Microporous Mesoporous Mater.*, 2008, **113**, 333–342.

51 X. C. Huang, L. B. Wu, J. F. Hsu, S. Shigeto and H. Y. Hsu, *Acta Biomater.*, 2015, **23**, 263–270.

52 D. Esquivel, J. Ouwehand, M. Meledina, S. Turner, G. Van Tendeloo, F. J. Romero-Salguero, J. De Clercq and P. Van Der Voort, *J. Hazard. Mater.*, 2017, **339**, 368–377.

53 N. V. Stolyarchuk, H. Kolev, M. Kanuchova, R. Keller, M. Vaclavikova and I. V. Melnyk, *Colloids Surf., A*, 2018, **538**, 694–702.

54 Q. Z. Zhou, H. F. Xiang, H. S. Fan, X. L. Yang, N. Zhao and J. Xu, *J. Mater. Chem.*, 2011, **21**, 13056–13061.

55 S. K. Lagergren, *K. Sven. Vetenskapsakad. Handl.*, 1898, **24**, 1–39.

56 Y. S. Ho, *J. Hazard. Mater.*, 2006, **136**, 681–689.

57 K. Chen, Z. Z. Zhang, K. Xia, X. J. Zhou, Y. F. Guo and T. Y. Huang, *ACS Omega*, 2019, **4**, 8568–8579.

58 J. G. Yu, Y. B. Yue, X. W. Wu, Q. Liu, F. P. Jiao, X. Y. Jiang and X. Q. Chen, *Environ. Sci. Pollut. Res.*, 2016, **23**, 5056–5076.